Influence of proton-skin thickness on the α decays of heavy nuclei

W. M. Seif[1;1)] A. Abdurrahman[2]

[1] Cairo University, Faculty of Science, Department of Physics, Giza, Egypt
[2] Misr University for Science and Technology (MUST), Faculty of Engineering, Department of Physics, Giza, Egypt

Abstract: We investigate the effect of proton-skin thickness on the α decay process. We consider 188 neutron-deficient nuclei belonging to the isotopic chains from Te ($Z=52$) to Pb ($Z=82$). The calculations of the half-life are carried out in the framework of the preformed cluster model, with the Wentzel-Kramers-Brillouin penetration probability and assault frequency. It is shown that the proton-skin thickness ($\Delta_{\rm p}$) of the daughter nucleus gives rise to a total α- daughter nucleus interaction potential of relatively wide deep internal pocket and a thinner Coulomb barrier of less height. This increases the penetration probability but decreases the assault frequency. The overall impact of the proton-skin thickness appears as a decrease in the decay half-life. The proton-skin thickness decreases the stability of the nucleus. The half-lives of the proton-skinned isotopes along the isotopic chain decrease exponentially with increasing the proton-skin thickness, whereas the Q_α-value increases with $\Delta_{\rm p}$. α-decay manifests itself as the second favorite decay mode of neutron-deficient nuclei, next to the β^+-decay and before proton-decay. It is indicated as main, competing, and minor decay mode, at 21%, 7%, and 57%, respectively, of the investigated nuclei.

Keywords: alpha decay, half-life, proton-skin thickness, branching ratio

PACS: 23.60.+e, 27.60.+j, 27.70.+q **DOI:** 10.1088/1674-1137/42/1/014106

1 Introduction

The neutron distributions in finite nuclei normally form a "neutron skin". Formation of proton skins is less likely than neutron skins [1]. In addition to the emergence of proton skins in proton-rich nuclei, the repulsive Coulomb interaction gives rise to a proton skin in neutron-deficient nuclei. The difference between the proton and neutron root-mean-square (rms) radii of nuclei simply indicates their proton-skin thickness. In some nuclei, the sharp radius of the proton distribution exceeds that of neutrons while the surface width is wider for neutrons than for protons [2]. The proton (neutron) skin thickness can also be defined as the difference between two limiting radii [1, 3]. The first radius is obtained when the ratio of the proton (neutron) density to the neutron (proton) density approaches a certain value (1% in Ref. [1]). The second radius is obtained when the proton (neutron) density turns into some percentage of the central density (1% in Ref. [1]). The proton (neutron) skin can be understood in terms of the equation of state of the asymmetric nuclear matter (ANM) and its pressure [4] as well as the density dependence of the nuclear symmetry energy [5, 6]. The pressure of ANM and neutron matter has been used to link the neutron skin in finite nuclei to the radius of neutron stars [7], and to other related observables. The impact of the proton skin on the structure, decays, and reactions of neutron-deficient and neutron-rich nuclei remains a matter of discussion.

Since the observation of α-decay by Rutherford and Geiger [8], and its subsequent interpretation by Gamow [9] as a quantum tunneling phenomenon, comprehensive experimental and theoretical studies have been performed on it to probe the nuclear structure. The exotic nuclei of extreme isospin asymmetries are of special interest. The study of such nuclei is relevant to the production of new exotic isotopes such as ^{63}Se, ^{67}Kr, ^{68}Kr, ^{59}Ge [10], ^{73}Mn, ^{76}Fe, ^{77,78}Co, ^{78,80,81,82}Ni, ^{83}Cu [11] and ^{178}Pb [12]. This also helps to investigate an expected island of α-emitters exhibiting short half-lives towards the $N=Z$ line and to estimate the borders of the proton-rich and neutron-deficient isotopes that could be produced in future experiments. The stability of nuclei is principally governed by the released energy and the change of the ground state properties from parent to daughter nuclei. For instance, the isospin asymmetry [13] and incompressibility [14] of nuclei, their deformation [15, 16], and the closed shell effect [17, 18] are essential factors affecting a possible decay mode. Also, the presence of unpaired nucleons in open shells [18, 19], the spin and parity assignments of these unpaired nucleons [20, 21], and the collective vibrational excitations [22] influence the com-

Received 12 September 2017, Published online 20 December 2017

1) E-mail: wseif@sci.cu.edu.eg

peting decay modes. These properties control the preformation probability of the emitted cluster inside the parent nucleus, the knocking frequency, the penetration probability, and finally the decay half-life [23, 24].

Recently, cluster radioactivity has been suggested as a way to correlate the neutron skin with the slope of symmetry energy [25], in the framework of the density-dependent cluster model. To do so, the density independent M3Y-Reid type of the nucleon-nucleon (NN) effective interaction, along with Fermi parameterizations of the proton and neutron density distributions, have been used. The results emphasized the previously reported direct proportionality of the density slope of symmetry energy to the thickness of the neutron skin. In a more recent work [26], a correlation is indicated between the change of neutron (proton) skin thickness, from parent to daughter nuclei, and the α-decay half-lives (T_α). It was shown that the observed T_α consistently follow the change in the neutron (proton) skin thickness after α-decays. It was indicated that the α-decays of nuclei with proton (neutron) skins preferably proceed to fulfill a significant decrease (very least increase) in the proton (neutron) skin thickness of their daughter nuclei. Explicitly, it was concluded that the neutron-skin thickness decreases the calculated T_α [27]. The effect of the proton-skin thickness on the α decays of neutron-deficient nuclei still needs further investigation.

In the present paper we address the impact of the proton skin thickness on the α decay processes. We focus on the neutron deficient nuclei in the trans-tin region of the nuclear chart. The observed decay modes from neutron-deficient and neutron-rich nuclei in the trans-tin region were considered in Ref. [21]. Here, we investigate both the observed decays of neutron-deficient nuclei and those that have not yet been observed. Among the decays considered here, 135 decay modes were not addressed in Ref. [21]. In the next section, we outline the methodology used to investigate the α-decay process in the framework of the preformed cluster model. Section 3 is devoted to a discussion of the effect of the proton skin thickness of both the parent and daughter nuclei on the α-decay process, as well as a detailed investigation of α decays of the neutron-deficient nuclei with mass numbers $105\leqslant A\leqslant 179$ ($52\leqslant Z\leqslant 82$). The paper ends with a brief summary and conclusions presented in Section 4.

2 Theoretical formalism

In the framework of the double folding model [28] we can calculate, respectively, the direct nuclear $V_{\rm N}(r,\theta)$ and the Coulomb $V_{\rm C}(r,\theta)$ parts of the interaction potential between an emitted α particle and a deformed daughter nucleus as,

$$V_{\rm N}(r,\theta) = \iint \big[\big(\rho_{\rm p\alpha}(\vec{r}_1)+\rho_{\rm n\alpha}(\vec{r}_1)\big)v_{00}(s=|\vec{r}+\vec{r}_2-\vec{r}_1|) \times(\rho_{\rm pD}(\vec{r}_2)+\rho_{\rm nD}(\vec{r}_2))+(\rho_{\rm p\alpha}(\vec{r}_1)-\rho_{\rm n\alpha}(\vec{r}_1)) \times v_{01}(s)(\rho_{\rm pD}(\vec{r}_2)-\rho_{\rm nD}(\vec{r}_2))\big]{\rm d}\vec{r}_1{\rm d}\vec{r}_2, \quad (1)$$

and

$$V_{\rm C}(r,\theta)=\iint \rho_{\rm p\alpha}(\vec{r}_1)v_{\rm C}(s)\rho_{\rm pD}(\vec{r}_2){\rm d}\vec{r}_1{\rm d}\vec{r}_2. \quad (2)$$

Here r(fm) defines the separation distance between the centers of mass of the interacting nuclei. θ represents the orientation angle of the emitted α-particle relative to the symmetry axis of the deformed daughter nucleus. s denotes the relative separation of the interacting nucleons belonging to the two nuclei. $\rho_{\rm p\alpha(D)}(\vec{r}_{1(2)})$ and $\rho_{\rm n\alpha(D)}(\vec{r}_{1(2)})$ are the proton and neutron density distributions of the α-particle (daughter nucleus), respectively. $v_{\rm C}$ represents the standard proton-proton Coulomb interaction, e^2/s. The M3Y type of the nucleon-nucleon interaction, with a zero-range exchange part, reads

$$v_{\rm N}(s,E)=v_{00}(s)+v_{01}(s)+\hat{j}_{00}\delta(s). \quad (3)$$

The strengths of the central isoscalar (v_{00}) and isovector (v_{01}) direct components of the M3Y effective interaction based on the G-matrix elements of the Reid [29] NN potential are given, respectively, as [30]

$$v_{00}(s)=7999.00\frac{{\rm e}^{-4s}}{4s}-2134.25\frac{{\rm e}^{-2.5s}}{2.5s}\ {\rm MeV}, \quad (4)$$

and

$$v_{01}(s)=-4885.5\frac{{\rm e}^{-4s}}{4s}+1175.5\frac{{\rm e}^{-2.5s}}{2.5s}\ {\rm MeV}. \quad (5)$$

To account for the single nucleon exchange term in an approximate form simpler than its finite range expression, the energy-dependent zero-range pseudopotential of the form [31]

$$\hat{J}_{00}(E)\approx -276\left[1-0.005\left(\frac{E}{A_\alpha}\right)\right]{\rm MeVfm}^3, \quad (6)$$

is widely used. Here, E/A_α represents the energy per nucleon of the emitted α-particle, corrected for the recoil energy of the daughter nucleus, $E=A_{\rm d}Q_\alpha/(A_\alpha+A_{\rm d})$. Q_α(MeV) defines the energy released in the decay. The detailed formalism used to perform the double-folding numerical calculations (Eqs. (1) and (2)) for spherical-deformed interacting nuclei, based on the Fourier transformation of the density and the multipole expansion method, is given in Refs. [32–34].

The neutron (proton) density distribution of a deformed nucleus can be described by the two-parameter Fermi shape,

$$\rho_{\rm n(p)}(r,\theta)=\rho_{0{\rm n(p)}}\left[1+e^{(r-R_{\rm n(p)}(\theta))/a_{\rm n(p)}}\right]^{-1}, \quad (7)$$

with the half-density radius

$$R_{\rm n(p)}(\theta)=R_{0{\rm n(p)}}\left[1+\sum_{i=2,3,4,6}\beta_i Y_{i0}(\theta)\right]. \quad (8)$$

β_i (i=2, 3, 4, 6) represent the multipole deformations of the nuclear density [35, 36]. For a nucleus of Z protons and N neutrons, the values of the radius $R_{0\mathrm{n(p)}}$ and diffuseness $a_{0\mathrm{n(p)}}$ parameters can be given as

$$\begin{aligned} R_{0\mathrm{n}}(\mathrm{fm})&=0.953N^{1/3}+0.015Z+0.774,\\ R_{0\mathrm{p}}(\mathrm{fm})&=1.322Z^{1/3}+0.007N+0.022,\\ a_{\mathrm{n}}(\mathrm{fm})&=0.446+0.072(N/Z),\\ a_{\mathrm{p}}(\mathrm{fm})&=0.449+0.071(Z/N). \end{aligned} \tag{9}$$

These expressions were obtained in a study [37] based on self-consistent Hartree-Fock (HF) calculations [38] using a Skyrme-SLy4 [39] effective NN interaction. The proton and neutron density distributions of the α-particle are also determined self-consistently [38]. The normalization of the neutron (proton) density to the number of neutrons (protons) gives the saturation density $\rho_{0\mathrm{n(p)}}$ in Eq. (7), $\int\rho_{\mathrm{n(p)}}(r,\theta)\mathrm{d}\vec{r}=N(Z)$. The rms radius $R^{\mathrm{rms}}_{\mathrm{n(p)}}$ of the neutron (proton) density distribution is obtained as

$$R^{\mathrm{rms}}_{\mathrm{n(p)}}=\left\langle R^2_{\mathrm{n(p)}}\right\rangle^{1/2}=\left(\frac{\int r^2_{\mathrm{n(p)}}\rho_{\mathrm{n(p)}}(\vec{r})\mathrm{d}\vec{r}}{\int\rho_{\mathrm{n(p)}}(\vec{r})\mathrm{d}\vec{r}}\right)^{1/2}. \tag{10}$$

The proton-skin thickness Δ_{p} can be expressed as the difference between the proton and neutron rms radii,

$$\Delta_{\mathrm{p}}(A,Z)=R^{\mathrm{rms}}_{\mathrm{p}}(A,Z)-R^{\mathrm{rms}}_{\mathrm{n}}(A,Z). \tag{11}$$

The ground state spin(J)-parity(π) assignment of the even(Z)-even(N) α-particle in its ground-state is $J^{\pi}_{\alpha}=0^{+}$. The unfavored α-decay modes from a parent nucleus in a state J^{π}_{P} to a daughter nucleus in a state $J^{\pi}_{\mathrm{D}}\neq J^{\pi}_{\mathrm{P}}$ require that the α-particle carries a non-zero angular momentum $\ell\neq0$. In this case, the conservation rules of angular momentum and parity imply

$$|J_{\mathrm{P}}-J_{\mathrm{D}}|\leqslant l\leqslant|J_{\mathrm{P}}+J_{\mathrm{D}}| \quad\text{and}\quad \pi_{\mathrm{P}}=\pi_{\mathrm{D}}(-1)^l. \tag{12}$$

Based on the principle of least action, the α-particle carries the minimum allowed value $\ell_{\min}$ that fulfills the conditions given by Eq. (12). For such unfavored decays, the centrifugal potential can be considered in its Langer form [40],

$$V_{\mathrm{l}}(r)=\frac{(l+1/2)^2\hbar^2}{2\mu r^2}. \tag{13}$$

This modified formulation, which replaces $\ell(\ell+1)$ by $(\ell+1/2)^2$, is commonly used to guarantee the proper physical behavior of the potential and the scattered radial wave function close to the origin [13,41]. $\mu=m_\alpha m_{\mathrm{D}}/(m_\alpha+m_{\mathrm{D}})$ is the reduced mass of the $\alpha(m_\alpha)$-daughter nucleus (m_{D}) system.

Based on Eqs. (1), (2) and (13), the α-daughter nucleus total potential V_{T} (r,θ) reads,

$$V_{\mathrm{T}}(r,\theta)=\lambda V_{\mathrm{N}}(r,\theta)+V_{\mathrm{C}}(r,\theta)+V_{\mathrm{l}}(r). \tag{14}$$

The renormalization factor λ is usually inserted into the nuclear part of the interaction potential to guarantee the α-core quasistationary state. λ is determined through the Bohr-Sommerfeld [42] and Wildermuth [43] quantization conditions.

Within the preformed cluster model arising from the Gamow picture of the tunneling decay process, the decay width $\Gamma(\theta)$ is obtained at a particular orientation angle θ, with respect to the axis of symmetry of the deformed daughter nucleus, as

$$\Gamma(\theta)=\hbar\nu(\theta)P(\theta). \tag{15}$$

Here ν (θ) and $P(\theta)$ define the assault frequency and the penetration probability of the α-particle across the Coulomb barrier, respectively. They can be obtained using the Wentzel-Kramers-Brillouin (WKB) approximation as

$$\nu(\theta)=\left[\int_{R_1(\theta)}^{R_2(\theta)}\frac{2\mu}{\hbar k(r,\theta)}\mathrm{d}r\right]^{-1}, \tag{16}$$

and

$$P(\theta)=\exp\left(-2\int_{R_2(\theta)}^{R_3}k(r,\theta)\mathrm{d}r\right). \tag{17}$$

The wave number $k(r,\theta)$ associated with the motion of the α-particle relative to the daughter nucleus is defined as

$$k(r,\theta)=\sqrt{\frac{2\mu}{\hbar^2}|V_{\mathrm{T}}(r,\theta)-Q_\alpha|}. \tag{18}$$

The three turning points $R_{i=1,2,3}$ (fm) of the WKB integrals (Eqs. (16) and (17)) are determined from the condition $V_{\mathrm{T}}(r,\theta)|_{r=R_i(\theta)}=Q_\alpha$. The orientation-independent [18] R_3, located at the far tail region of the long-range Coulomb potential V_{C} (r,θ), can be obtained in terms of the atomic number of the daughter nucleus (Z_{d}) and the angular momentum carried by the α-particle (ℓ) as [16],

$$R_3=\frac{1.44Z_{\mathrm{d}}}{Q_\alpha}+\sqrt{\left(\frac{1.44Z_{\mathrm{d}}}{Q_\alpha}\right)^2+\frac{l(l+1)\hbar^2}{2\mu Q_\alpha}}, \tag{19}$$

The orientation-dependent decay width, Eq. (15), is then averaged over the orientation angle θ,

$$\Gamma=\frac{1}{2}\int_0^\pi\Gamma(\theta)\sin\theta\mathrm{d}\theta. \tag{20}$$

Finally, the half-life of the parent nucleus against α-decay reads

$$T_\alpha=\frac{\hbar\ln2}{S\Gamma}, \tag{21}$$

where S denotes the preformation probability of the particle in the parent nucleus. Using Eq. (21), one can estimate the preformation probability using the observed partial half-life T^{exp}_α and the calculated decay width Γ. Based on the experimentally extracted S^{exp}_α for different decay modes of hundreds of α-emitters [18, 20, 21],

an empirical formula has been proposed to estimate the α-preformation factor in terms of the nucleonic shell closures (Z_0, N_0) in the parent nucleus (Z, N) as

$$
\begin{aligned}
S_\alpha &= \frac{\mathcal{A}\mathrm{e}^{-0.003(Z-Z_0-Z_\mathrm{c})^2}\mathrm{e}^{-0.006(N-N_0-N_\mathrm{c})^2}-a_\mathrm{p}}{a_\mathrm{l}},\\
a_\mathrm{l} &= \frac{A^2}{3190\sqrt{l_\mathrm{min}}}-a_\mathrm{l}0, \quad a_\mathrm{l0}=\begin{cases}3.9 & \text{for } A\geqslant 154\\ 1.0 & \text{for } A<154\end{cases}, \quad a_\mathrm{l}=1 \text{ for } l_\mathrm{min}=0,\\
a_\mathrm{p} &= \begin{cases}0.0040(Z-Z_0)^{1/3} & \text{for odd}(Z)\text{-even}(N) \text{ nuclei}\\ 0.0056(N-N_0)^{1/3} & \text{for even}(Z)\text{-odd}(N) \text{ nuclei}\\ 0.0088(Z-Z_0+N-N_0)^{1/3} & \text{for odd}(Z)\text{-odd}(N) \text{ nuclei}\end{cases}
\end{aligned}
\tag{22}
$$

Z_C and N_C define, respectively, the numbers of protons and neutrons exceeding the shell closures (Z_0,N_0), at which S_α reaches a local maximum. The dimensionless parameter $A(Z_0,N_0)$ correlates with the shell closures. a_p [18] and a_ℓ [20] account for the pairing effect and the hindrance in S_α due to the difference in the spinparity of the nuclei involved in the unfavored decays, respectively. The adopted fitting values [21] of Z_C, N_C and A for the shell closure combinations used in the present work are listed in Table 1.

Table 1. Optimized fitting parameters of the empirical formula of the α preformation factor (Eq. (22)) for nuclei with extra nucleons outside the shell closures, (Z_0,N_0) = (50, 50), (50, 70), (50, 82), (70, 70), (70, 82), (70, 102) and (82, 82), as obtained from the fit for the experimentally estimated S_α^exp of the observed decay modes investigated in Refs. [18, 20, 21] and in the present work. The fit parameters for the shell closure sets (Z>82, N>82) are given in Ref. [21].

Z_0	N_0	Z_c	N_c	A
50	50	8	8	0.087
	70		6	0.100
	82		8	0.110
70	70	6	6	0.080
	82		8	0.063
	102		12	0.050
82	82	12	8	0.073

3 Results and discussion

In the present study we restrict our attention to the ground-state to ground-state α-decays of neutron-deficient nuclei in the region of mass number A =105–179. The 188 parent nuclei investigated have atomic numbers Z =52–82 (N =53–97). We consider both decays that have already been experimentally observed and those that have not been observed yet. We investigate whether the proton skin enhances or hinders the α-decay process.

Figure 1 shows the effect of the proton-skin thickness on the α-core interaction potential. Presented in Figs. 1(a), 1(b) and 1(c), respectively, are the nuclear, Coulomb and the total scattering potential of the interacting α+^{101}Sn nuclei. This nuclear system participates in the α-decay of the ^{105}Te nucleus (Q_α =5.069±0.003 MeV [44], T_α =0.633±0.066 μs [45]). ^{101}Sn is almost a spherical nucleus [35]. The self-consistent HF calculations based on the SK255 [46], SLy4 [39], SII [47], ZR1(x_0=0.1) [48] and ZR1(x_0=0.024) parameterizations of the Skyrme Energy Density Functional (EDF) yields Δ_p(^{101}Sn)=0.007–0.065 fm. The obtained proton and neutron density distributions of ^{101}Sn have been used in the calculations presented in Fig. 1. While the rms radius of the proton density distributions based on the mentioned forces ranges from 4.356 fm to 4.453 fm, the neutron rms radius ranges from 4.349 fm to 4.409 fm. We examined more than 30 popular parameterizations of the Skyrme EDF. Most of them give Δ_p around the value obtained by the Skyrme-SLy4 interaction, Δ_p=0.065 fm. As shown in Fig. 1(a), increasing the proton-skin thickness increases the attractive nuclear part in its inner region, but reduces it in the overlap-density region. The attractive nuclear potential slightly increases again with Δ_p in the surface and Coulomb barrier regions. While the slight changes in the neutron and proton rms radii affect the short-range attractive nuclear potential, the long-range repulsive Coulomb potential remains unaffected, as seen in Fig. 1(b). The influence of the larger Δ_p on the nuclear part of the potential results in a decreased total potential, Figs. 1(c). For comparison, we present in Fig. 1(d) the calculated total potentials based on the above-mentioned Skyrme NN interactions. The potential based on a Skyrme effective interaction is characterized by a repulsive core giving rise to a pocket being formed in the inner part of the potential. The internal pocket of the total potential based on M3Y-type interactions is commonly obtained after introducing the renormalization factor λ (Eq. (14)) to the nuclear part of the potential. As shown in Fig. 1(d), larger Δ_p produces a

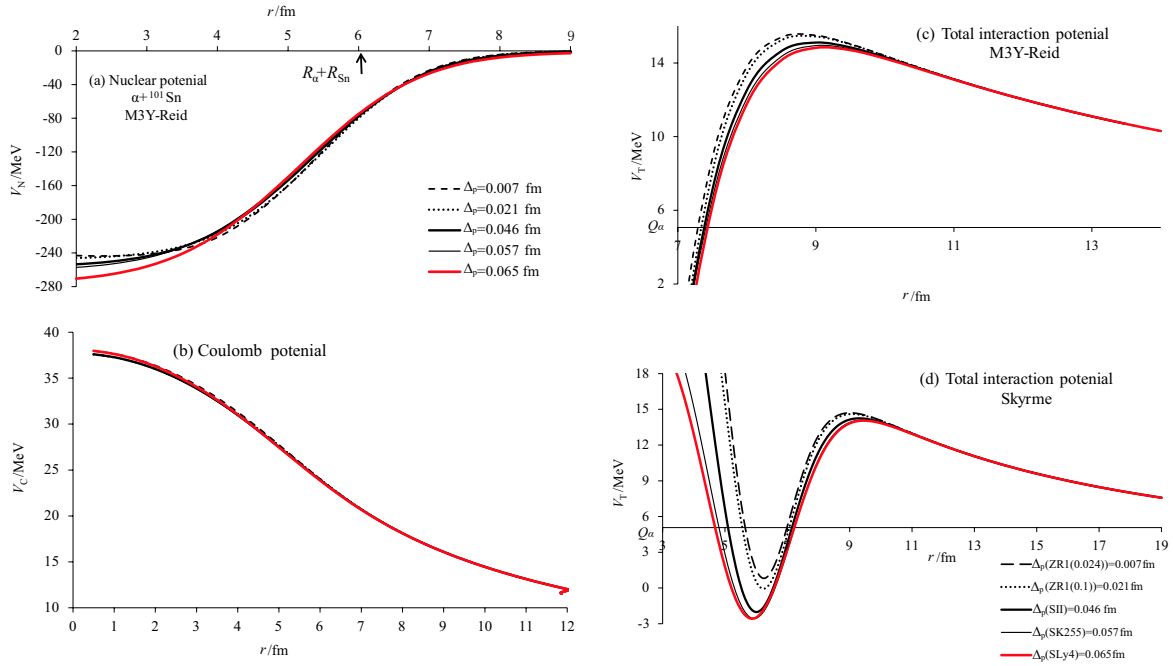

Fig. 1. (color online) The radial dependence of the (a) nuclear, (b) Coulomb and (c) total interaction potential between α and ^{101}Sn nuclei, which are involved in the α decay of ^{105}Te, at different values of the proton-skin thickness ($\Delta_{\rm p}$) of ^{101}Sn. The nuclear part is computed in terms of the M3Y-Reid effective NN interaction, Eqs. (4, 5 and 6). The proton and neutron density distributions of ^{101}Sn with different $\Delta_{\rm p}$ are obtained from self-consistent HF calculations based on the SK255, SLy4, SII, ZR1(x_0=0.1) and ZR1(x_0=0.024) parameterizations of the Skyrme EDF. The arrow indicates the sum of the average rms radii of the interacting nuclei. (d) The total interaction potential based on the mentioned Skyrme NN interactions.

wider and deeper internal pocket. Most importantly, $\Delta_{\rm p}$ lowers the height of the Coulomb barrier, shifting it to larger internuclear distance, as shown in Figs. 1(c) and 1(d). The Coulomb barrier width decreases with $\Delta_{\rm p}$. The position of the third turning point R_3, that located in the extreme outer region of the potential, does not depend on the density distribution of the participating protons but only on their numbers (Z_α and $Z_{\rm D}$), Eq. (19).

Figures 2(a)–2(c) show, respectively, the dependence of the α penetration probability P, its assault frequency ν (s^{-1}), and the calculated partial half-life T_α (μs) of ^{105}Te on the proton-skin thickness of the ^{101}Sn daughter nucleus. Figure 2(a) shows that P increases with $\Delta_{\rm p}$. This is understood as a consequence of decreasing both the Coulomb barrier height and its width with $\Delta_{\rm p}$, Fig. 1(c). The penetration probability increases with decreasing the area under the Coulomb barrier, Eqs. (17) and (18). On the other hand, the assault frequency decreases with $\Delta_{\rm p}$ as shown in Fig. 2(b). This is expected since the internal pocket width $R_{21}=R_2-R_1$ increases with $\Delta_{\rm p}$. The assault frequency is defined as the inverse of the time taken to traverse this distance back and forth, Eq. (16). The obtained increase of P with $\Delta_{\rm p}$ is more influential in the decay process than the decrease of ν. The overall effect is that $\Delta_{\rm p}$ reduces the half-life of the nucleus against α-decay, Fig. 2(c). A preformation factor of 0.0591 (Eq. (22) with $\ell_{\rm min}$ =0) has been used in calculations of T_α in Fig. 2(c). Indeed, the α-preformation factor (Eq. (21)) that can be extracted from the experimental T_α and the calculated decay width will be affected by the considered value of $\Delta_{\rm p}$. A larger proton-skin thickness would indicate a lower estimated preformation factor, due to lower calculated half-life.

Figure 3 displays the influence of the proton-skin thickness on the half-life against α-decay and the released energy along the same isotopic chain. Shown in Figs. 3(a) and 3(b), respectively, are the Q_α-values [44] and the partial half-lives T_α (on a logarithmic scale) of the proton-skinned isotopes of Te, Cs and Ba, as functions of their proton-skin thickness given by Eqs. (9)–(11). The experimentally observed T_α of the $^{105-110}$Te, ^{112,114}Cs and ^{114}Ba isotopes are represented in Fig. 3 by solid symbols. The calculated T_α of ^{111}Te, $^{113,115-118}$Cs and $^{113,115-120}$Ba, in which no α-decays have been observed, are represented by open symbols. As seen in Fig. 3(a), for the same isotopic chain, Q_α linearly increases with $\Delta_{\rm p}$. The half-lives of the proton-skinned nuclei decrease exponentially with increasing proton-skin thickness, Fig. 3(b). The pairing effect slightly influences Q_α and T_α, keeping their general

trends with $\Delta_{\rm p}$. As clearly seen in Figs. 2(c), 3(a) and 3(b), the overall conclusion is that the proton-skin thickness is a good indicator for the stability of the nucleus. $\Delta_{\rm p}$ makes the nucleus less stable.

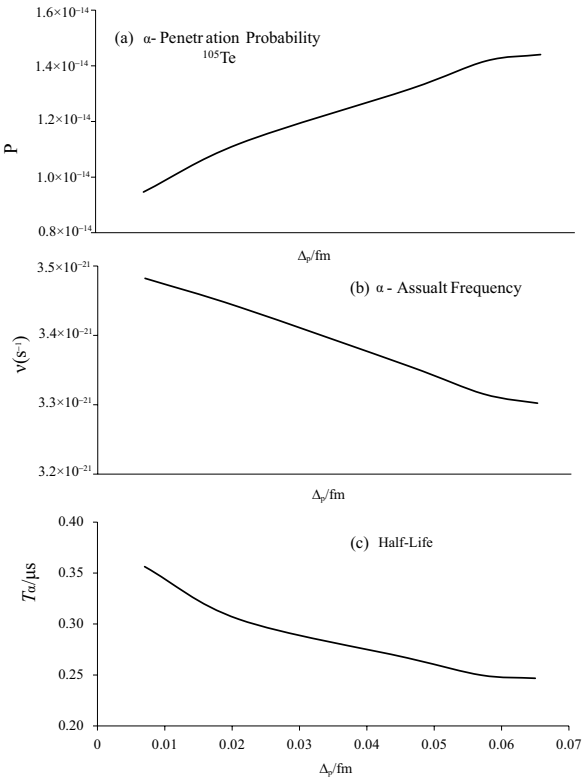

Fig. 2. (a) the α-penetration probability, (b) the assault frequency, and (c) the calculated partial half-life T_α of the ground-state to ground-state α decay of ^{105}Te, as functions of the proton-skin thickness of the daughter nucleus ^{101}Sn. The preformation factor S_α=0.0591 (Eq. (22)) is considered in the calculations of T_α in panel (c).

Table 2 gives the calculated partial half-lives $T_\alpha^{\rm cal}$ (column 9) of the ground-state to ground-state decays of the neutron-deficient nuclei of $52 \leqslant Z \leqslant 82$. The presented parent nuclei show calculated proton-skin thickness $\Delta_{\rm p}>0$. The third and fourth columns in Table 2 contain the ground-state spin and parity ($J^\pi_{\rm P(D)}$) of the parent (P) and daughter (D) nuclei listed in the first and second columns, respectively. The minimum values of angular momentum $\ell_{\rm min}$ carried out by the α-particle in allowed decays are shown in the fifth column. Given in columns 6 and 7, respectively, are the proton-skin thickness of the parent and daughter nuclei as calculated using the self-consistent HF method [37,38], based on the Skyrme-SLy4 NN interaction. Listed in the eighth column is the released energy Q_α in MeV [44]. Concerning the 188 investigated decay modes in Table 2, 59 decays have been experimentally observed and quantified [45,49]. The experimental half-lives $T_\alpha^{\rm exp}$ (s) of these observed decays are listed in the tenth column. The calculated branching ratios, $B_{\rm cal}(\%)=(T_\alpha^{\rm cal}/\text{experimental total half-life of the nucleus})\times 100$, for the α-decays that have not yet been observed, are given in the last column.

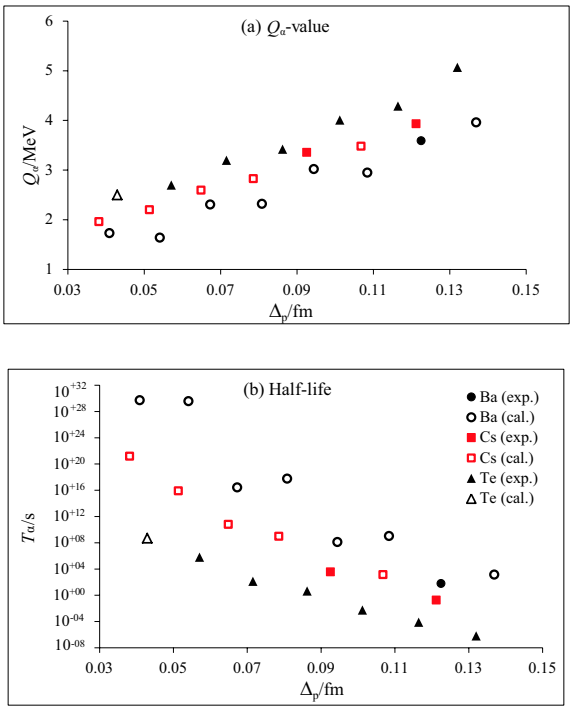

Fig. 3. (color online) (a) The Q_α-values [44] and (b) the observed partial half-lives (T_α) of the proton-skinned Te, Cs and Ba α-emitter isotopes and the calculated T_α of the corresponding isotopes that have no observed α-decays yet, as a function of the proton-skin thickness ($\Delta_{\rm p}$) of the parent nuclei. T_α is plotted on a logarithmic scale.

The ground-state multipole deformations ($\beta_{2,3,4,6}$) of the deformed daughter nuclei are taken into accounts in our calculations [35, 36]. The preformation factors are deduced using the semi-empirical formula given in Eq. (22). α-decay was observed as the main decay mode for 38 neutron-deficient nuclei [45, 49]. Most of these nuclei have even proton number. α-decay was observed as a competing (minor) decay mode for 9 (12) neutron-deficient nuclei. The other decay modes that have been observed for these 59 neutron-deficient nuclei are the β^+ (49 nuclei) and proton (10 nuclei) decays [45]. As shown in Table 2, the calculated partial half-lives are in good agreement with the observed ones. For most of the observed decays, the calculated T_α and the observed half-life are of the same order of magnitude. They differ by one or two orders of magnitude for a few decays. This suggests that using the parameterization of the empirical formula (22) given in Table 2 in the present calculations is trustworthy, even although it was determined using

Table 2. The calculated partial half-lives $T_\alpha^{\rm cal}$ (Eq. (21)), column 9, against ground-state to ground state α-decays of the neutron-deficient parent nuclei (column 1) that have non-vanishing calculated proton skin-thickness. The deformations of daughter nuclei are taken into account. The semiempirical formula (22) has been used to estimate the α-preformation probability. Columns 2-5 identify, respectively, the daughter nuclei, the ground-state spin and parity $J^\pi_{\rm P(D)}$ of the parent P and daughter D nuclei [45], and the minimum allowed value $\ell_{\rm min}$ of the angular momentum carried away by the emitted α-particle. The square brackets [ ] and parentheses ( ) are used to indicate the non-experimental spin-parity assignments and uncertain values [45], respectively. The proton-skin thickness (Eq. (11)) of the parent and daughter nuclei calculated self-consistently using the HF method based on Skyrme-SLy4 NN interactions are listed in columns 6 and 7, respectively. The values of the energy released in the decays (Q_α) are given in Column 8. Q_α-values partly derived from trends in the mass surface [44], with uncertainty fixed at 0.05 MeV, are indicated in square brackets. The experimentally observed half-lives ($T_\alpha^{\rm exp}$) are given in column 10. In the last column we show the calculated percentage branching ($B_{\rm cal}$ (%)) for the decays that have not been observed yet. The uncertainties in the calculated partial half-life and in the experimental total half-life of the nucleus were both considered in the estimated branching ratios.

parent	daughter	$J^\pi_{\rm P}$ [45]	$J^\pi_{\rm D}$ [45]	$\ell_{\rm min}$	$\Delta_{\rm p}$(P)/fm	$\Delta_{\rm p}$(D)/fm	Q_α/MeV [44]	$T_\alpha^{\rm cal}$/s	$T_\alpha^{\rm exp}$/s [45]	$B_{\rm cal}$(%)
^{105}Te	^{101}Sn	$(7/2^+)$	$(7/2^+)$	0	0.075	0.065	5.069±0.003	(2.37±0.058)×10^{-7}	(6.330±0.660)×10^{-7}	
^{106}Te	^{102}Sn	0^+	0^+	0	0.062	0.051	4.290±0.009	(25.550±2.510)×10^{-5}	(7.800±1.100)×10^{-5}	
^{107}Te	^{103}Sn	$[5/2^+]$	$[5/2^+]$	0	0.049	0.037	4.008±0.005	(6.206±0.358)×10^{-3}	(5.500±2.500)×10^{-3}	
^{108}Te	^{104}Sn	0^+	0^+	0	0.036	0.024	3.420±0.008	12.130±1.371	4.331±0.558	
^{109}Te	^{105}Sn	$(5/2^+)$	$(5/2^+)$	0	0.024	0.012	3.198±0.006	(4.469±0.422)×10^{2}	(1.356±0.529)×10^{2}	
^{110}Te	^{106}Sn	0^+	0^+	0	0.013	0	2.699±0.008	(46.080±7.621)×10^{5}	(6.200±0.267)×10^{5}	
^{111}Te	^{107}Sn	$(5/2)^+$	$(5/2^+)$	0	0.002	−0.012	2.500±0.008	(4.982±0.992)×10^{8}		(5.5±1.2)×10^{-6}
^{107}I	^{103}Sb	$[5/2^+]$	$[5/2^+]$	0	0.079	0.071	[4.324±0.050]	(7.568±3.678)×10^{-4}		3.5±1.7
^{108}I	^{104}Sb	$[1^+]$		0	0.066	0.058	4.100±0.050	(0.958±0.499)×10^{-2}	(3.956±0.659)×10^{-2} [49]	
^{109}I	^{105}Sb	$1/2^+$	$(5/2^+)$	2	0.054	0.045	3.918±0.021	0.229±0.058	0.812±0.268	
^{110}I	^{106}Sb	(1^+)	(2^+)	2	0.041	0.031	3.580±0.050	26.390±16.142	4.057±0.857	
^{111}I	^{107}Sb	$[5/2^+]$	$[5/2^+]$	0	0.029	0.019	3.275±0.005	(0.503±0.043)×10^{3}	(2.500±0.200)×10^{3}	
^{112}I	^{108}Sb	$[1^+]$	(4^+)	4	0.017	0.007	2.957±0.012	(26.170±5.751)×10^{5}	(2.783±0.067)×10^{5}	
^{113}I	^{109}Sb	$[5/2^+]$	$[5/2^+]$	0	0.007	−0.004	2.707±0.010	(0.227±0.047)×10^{8}	(1.994±0.060)×10^{9}	
^{109}Xe	^{105}Te	$[7/2^+]$	$(7/2^+)$	0	0.082	0.075	4.217±0.007	(0.732±0.060)×10^{-2}	(1.300±0.200)×10^{-2}	
^{110}Xe	^{106}Te	0^+	0^+	0	0.069	0.062	3.872±0.009	0.364±0.044	0.211±0.120	
^{111}Xe	^{107}Te	$[5/2^+]$	$[5/2^+]$	0	0.057	0.049	3.720±0.050	3.595±2.137	7.725±3.334	
^{112}Xe	^{108}Te	0^+	0^+	0	0.045	0.036	3.330±0.006	(7.979±0.809)×10^{2}	(4.850±3.900) ×10^{2}	
^{113}Xe	^{109}Te	$[5/2^+]$	$(5/2^+)$	0	0.033	0.024	3.087±0.008	(5.991±0.832)×10^{4}	(2.491±0.073) ×10^{4}	
^{114}Xe	^{110}Te	0^+	0^+	0	0.022	0.013	2.719±0.013	(8.345±2.334)×10^{7}		(1.3±0.4)×10^{-5}
^{115}Xe	^{111}Te	$(5/2^+)$	$(5/2)^+$	0	0.011	0.002	2.506±0.014	(1.518±0.503)×10^{10}	(7.250±3.750) ×10^{6}	
^{116}Xe	^{112}Te	0^+	0^+	0	0.001	−0.009	2.096±0.016	(1.797±0.845)×10^{15}		(4.3±2.1)×10^{-12}
^{112}Cs	^{108}I	$[1^+]$	$[1^+]$	0	0.074	0.066	3.930±0.120	1.825±1.674	0.189±0.014	
^{113}Cs	^{109}I	$(3/2^+)$	$1/2^+$	2	0.061	0.054	3.483±0.008	(1.406±0.168)×10^{3}		(1.3±0.2)×10^{-6}
^{114}Cs	^{110}I	(1^+)	(1^+)	0	0.049	0.041	3.360±0.050	(7.473±5.037)×10^{3}	(3.604±1.313)×10^{3}	
^{115}Cs	^{111}I	$[9/2^+]$	$[5/2^+]$	2	0.037	0.029	[2.830±0.050]	(3.348±2.637)×10^{8}		(1.6±1.5)×10^{-6}
^{116}Cs	^{112}I	(1^+)	$[1^+]$	0	0.026	0.017	[2.600±0.050]	(1.909±1.599)×10^{10}		(1.3±1.1)×10^{-8}
^{117}Cs	^{113}I	$[9/2^+]$	$[5/2^+]$	2	0.015	0.007	2.200±0.060	(8.228±7.910)×10^{15}		(1.4±1.3)×10^{-12}
^{118}Cs	^{114}I	2	1+	1	0.005	−0.004	[1.960±0.050]	(1.513±0.756)×10^{21}		<10^{-15}

Continued on next page

Table 2. – continued from previous page

parent	daughter	$J^{\pi}_{\rm P}$ [45]	$J^{\pi}_{\rm D}$ [45]	$\ell_{\rm min}$	$\Delta_{\rm p}$(P)/fm	$\Delta_{\rm p}$(D)/fm	Q_α/MeV [44]	$T^{\rm cal}_\alpha$/s	$T^{\rm exp}_\alpha$/s [45]	$B_{\rm cal}$(%)
^{113}Ba	^{109}Xe	$[5/2^+]$	$[7/2^+]$	2	0.089	0.082	[3.960±0.050]	8.735±4.976		1.7±1.0
^{114}Ba	^{110}Xe	0^+	0^+	0	0.075	0.069	3.592±0.019	256.600±69.700	62.708±34.792	
^{115}Ba	^{111}Xe	$[5/2^+]$	$[5/2^+]$	0	0.063	0.057	[2.950±0.050]	$(3.062\pm2.352)\times10^{7}$		$(3.9\pm3.2)\times10^{-6}$
^{116}Ba	^{112}Xe	0^+	0^+	0	0.052	0.045	[3.020±0.050]	$(6.339\pm4.774)\times10^{6}$		$(5.3\pm4.3)\times10^{-5}$
^{117}Ba	^{113}Xe	$(3/2)^{[+]}$	$[5/2^+]$	2	0.040	0.033	[2.320±0.050]	$(9.313\pm8.372)\times10^{14}$		$(1.0\pm0.9)\times10^{-12}$
^{118}Ba	^{114}Xe	0^+	0^+	0	0.030	0.022	[2.310±0.050]	$(2.542\pm2.291)\times10^{14}$		$(1.1\pm1.0)\times10^{-11}$
^{119}Ba	^{115}Xe	$(5/2^+)$	$(5/2^+)$	0	0.019	0.011	[1.640±0.050]	$(8.105\pm7.992)\times10^{25}$		$<10^{-15}$
^{120}Ba	^{116}Xe	0^+	0^+	0	0.009	0.001	[1.730±0.050]	$(7.500\pm7.346)\times10^{23}$		$<10^{-15}$
^{117}La	^{113}Cs	$(3/2^+)$	$(3/2^+)$	0	0.065	0.061	[2.870±0.050]	$(8.894\pm7.058)\times10^{8}$		$(7.0\pm5.8)\times10^{-9}$
^{118}La	^{114}Cs		(1^+)	0	0.054	0.049	[2.700±0.050]	$(4.567\pm3.789)\times10^{10}$		$(1.4\pm1.2)\times10^{-9}$
^{119}La	^{115}Cs	$[11/2^-]$	$[9/2^+]$	1	0.043	0.037	[2.490±0.050]	$(4.485\pm3.916)\times10^{13}$		$(9.4\pm8.2)\times10^{-12}$
^{120}La	^{116}Cs		(1^+)	0	0.033	0.026	[2.050±0.050]	$(1.419\pm1.344)\times10^{19}$		$<10^{-15}$
^{121}La	^{117}Cs	$[11/2^-]$	$[9/2^+]$	1	0.022	0.015	[1.880±0.050]	$(5.751\pm5.567)\times10^{22}$		$<10^{-15}$
^{122}La	^{118}Cs		2	0	0.012	0.005	[1.440±0.050]	$(1.618\pm1.611)\times10^{32}$		$<10^{-15}$
^{123}La	^{119}Cs	$[11/2^-]$	$9/2^+$	1	0.002	−0.005	[1.230±0.050]	$(4.234\pm4.230)\times10^{39}$		$<10^{-15}$
^{119}Ce	^{115}Ba	$[5/2^+]$	$[5/2^+]$	0	0.067	0.063	[2.660±0.050]	$(6.388\pm5.397)\times10^{11}$		$(1.1\pm0.9)\times10^{-10}$
^{120}Ce	^{116}Ba	0^+	0^+	0	0.057	0.052	[2.560±0.050]	$(7.393\pm6.395)\times10^{12}$		$(1.3\pm1.2)\times10^{-11}$
^{121}Ce	^{117}Ba	$(5/2)^{[+]}$	$(3/2)^{[+]}$	2	0.046	0.040	[2.340±0.050]	$(2.046\pm1.852)\times10^{16}$		$(3.2\pm3.0)\times10^{-14}$
^{122}Ce	^{118}Ba	0^+	0^+	0	0.036	0.030	[2.060±0.050]	$(6.678\pm6.342)\times10^{19}$		$<10^{-15}$
^{123}Ce	^{119}Ba	$(5/2)^{[+]}$	$(5/2^+)$	0	0.025	0.019	[1.880±0.050]	$(1.205\pm1.170)\times10^{23}$		$<10^{-15}$
^{124}Ce	^{120}Ba	0^+	0^+	0	0.015	0.009	[1.550±0.050]	$(2.115\pm2.100)\times10^{30}$		$<10^{-15}$
^{125}Ce	^{121}Ba	$(7/2^-)$	5/2(+)	1	0.006	−0.001	[1.660±0.050]	$(2.721\pm2.686)\times10^{28}$		$<10^{-15}$
^{121}Pr	^{117}La	(3/2)	$(3/2^+)$	0	0.070	0.065	[2.620±0.050]	$(7.898\pm6.771)\times10^{12}$		$(7.8\pm7.3)\times10^{-13}$
^{122}Pr	^{118}La			0	0.058	0.054	[2.360±0.050]	$(2.121\pm1.924)\times10^{16}$		$(1.3\pm1.2)\times10^{-14}$
^{123}Pr	^{119}La	$[3/2^+]$	$[11/2^-]$	5	0.048	0.043	[2.140±0.050]	$(1.969\pm1.856)\times10^{21}$		$<10^{-15}$
^{124}Pr	^{120}La			0	0.038	0.033	[1.990±0.050]	$(1.005\pm0.965)\times10^{22}$		$<10^{-15}$
^{125}Pr	^{121}La	$[3/2^+]$	$[11/2^-]$	5	0.028	0.022	[1.830±0.050]	$(9.174\pm8.967)\times10^{26}$		$<10^{-15}$
^{126}Pr	^{122}La	(4)		0	0.017	0.012	[1.800±0.050]	$(9.181\pm8.993)\times10^{25}$		$<10^{-15}$
^{127}Pr	^{123}La	$[3/2^+]$	$[11/2^-]$	5	0.008	0.002	[1.680±0.050]	$(1.587\pm1.566)\times10^{30}$		$<10^{-15}$
^{124}Nd	^{120}Ce	0^+	0^+	0	0.060	0.057	[2.650±0.050]	$(2.399\pm2.059)\times10^{13}$		$(7.9\pm6.8)\times10^{-12}$
^{125}Nd	^{121}Ce	$(5/2)^{[+]}$	$(5/2)^{[+]}$	0	0.049	0.046	[2.670±0.050]	$(2.100\pm1.796)\times10^{13}$		$(1.4\pm1.3)\times10^{-11}$
^{126}Nd	^{122}Ce	0^+	0^+	0	0.040	0.036	[2.460±0.050]	$(6.529\pm5.843)\times10^{15}$		$(7.7\pm6.9)\times10^{-14}$
^{127}Nd	^{123}Ce	$[5/2^+]$	$(5/2)^{[+]}$	0	0.029	0.025	[2.330±0.050]	$(5.653\pm5.185)\times10^{17}$		$(2.4\pm2.3)\times10^{-15}$
^{128}Nd	^{124}Ce	0^+	0^+	0	0.019	0.015	[2.180±0.050]	$(5.406\pm5.080)\times10^{19}$		$<10^{-15}$
^{129}Nd	^{125}Ce	$[5/2^+]$	$(7/2^-)$	1	0.010	0.006	[1.920±0.050]	$(2.138\pm2.075)\times10^{25}$		$<10^{-15}$
^{130}Nd	^{126}Ce	0^+	0^+	0	0.001	−0.005	1.800±0.040	$(1.681\pm1.598)\times10^{26}$		$<10^{-15}$
^{126}Pm	^{122}Pr			0	0.062	0.058	[3.010±0.050]	$(4.303\pm4.415)\times10^{10}$		$(3.1\pm2.5)\times10^{-9}$
^{127}Pm	^{123}Pr	$[5/2^+]$	$[3/2^+]$	2	0.051	0.048	[3.020±0.050]	$(1.548\pm1.225)\times10^{11}$		$(1.7\pm1.4)\times10^{-9}$
^{128}Pm	^{124}Pr	$(5,6,7)^{[+]}$		0	0.041	0.038	[2.940±0.050]	$(2.591\pm2.091)\times10^{11}$		$(1.4\pm1.2)\times10^{-9}$
^{129}Pm	^{125}Pr	$(5/2^-)$	$[3/2^+]$	1	0.031	0.028	[2.630±0.050]	$(2.373\pm2.059)\times10^{15}$		$(5.4\pm5.1)\times10^{-13}$

Continued on next page

Table 2. – continued from previous page

parent	daughter	$J^{\pi}_{\rm P}$ [45]	$J^{\pi}_{\rm D}$ [45]	$\ell_{\rm min}$	$\Delta_{\rm p}$(P)/fm	$\Delta_{\rm p}$(D)/fm	Q_α/MeV [44]	$T^{\rm cal}_\alpha$/s	$T^{\rm exp}_\alpha$/s [45]	$B_{\rm cal}$(%)
^{130}Pm	^{126}Pr	(4^+)	(4,5,6)	0	0.022	0.017	[2.500±0.050]	(3.624±3.232)×10^{16}		(3.7±3.4)×10^{-14}
^{131}Pm	^{127}Pr	$(11/2^-)$	$[3/2^+]$	5	0.012	0.008	[2.460±0.050]	(2.082±1.875)×10^{18}		(1.8±1.7)×10^{-15}
^{132}Pm	^{128}Pr	(3^+)	(3^+)	0	0.003	0.002	[2.280±0.050]	(1.053±0.978)×10^{19}		<10^{-15}
^{128}Sm	^{124}Nd	0^+	0^+	0	0.063	0.060	[3.430±0.050]	(2.989±2.138)×10^{7}		(3.4±2.5)×10^{-6}
^{129}Sm	^{125}Nd	$(1/2^+)$	$(5/2)^{[+]}$	2	0.053	0.049	[3.170±0.050]	(3.811±2.923)×10^{10}		(4.0±3.3)×10^{-9}
^{130}Sm	^{126}Nd	0^+	0^+	0	0.043	0.040	[3.060±0.050]	(5.533±4.366)×10^{10}		(4.8±3.8)×10^{-9}
^{131}Sm	^{127}Nd	$[5/2^+]$	$[5/2^+]$	0	0.033	0.029	[2.980±0.050]	(6.761±5.451)×10^{11}		(5.8±4.9)×10^{-10}
^{132}Sm	^{128}Nd	0^+	0^+	0	0.024	0.019	[2.810±0.050]	(1.199±1.007)×10^{13}		(1.2±1.0)×10^{-10}
^{133}Sm	^{129}Nd	$(5/2^+)$	$[5/2^+]$	0	0.015	0.010	[2.660±0.050]	(6.122±5.318)×10^{14}		(2.0±1.8)×10^{-12}
^{134}Sm	^{130}Nd	0^+	0^+	0	0.006	0.001	[2.800±0.050]	(1.216±1.024)×10^{13}		(2.9±2.5)×10^{-10}
^{130}Eu	^{126}Pm	(1^+)		0	0.064	0.062	[3.240±0.050]	(1.104±0.839)×10^{10}		(2.8±2.5)×10^{-11}
^{131}Eu	^{127}Pm	$3/2^+$	$[5/2^+]$	2	0.054	0.051	[3.090±0.050]	(6.188±4.892)×10^{11}		(8.3±6.9)×10^{-12}
^{132}Eu	^{128}Pm		$(5)^{[+]}$	0	0.044	0.041	[3.160±0.050]	(1.030±0.800)×10^{11}		(2.5±1.9)×10^{-10}
^{133}Eu	^{129}Pm	$[11/2^-]$	$(5/2^-)$	4	0.035	0.031	[3.220±0.050]	(1.274±0.976)×10^{11}		(3.8±2.9)×10^{-10}
^{134}Eu	^{130}Pm		(4^+)	0	0.026	0.022	[3.040±0.050]	(2.772±2.218)×10^{11}		(6.6±6.0)×10^{-10}
^{135}Eu	^{131}Pm	[11/2-]	(11/2-)	0	0.016	0.012	[3.090±0.050]	(8.708±6.888)×10^{10}		(5.1±4.3)×10^{-9}
^{136}Eu	^{132}Pm	(7^+)	(3^+)	4	0.007	0.003	[2.960±0.050]	(3.892±3.183)×10^{13}		(2.8±2.3)×10^{-11}
^{133}Gd	^{129}Sm	$[5/2^+]$	$(1/2^+)$	2	0.056	0.053	[3.720±0.050]	(6.275±4.248)×10^{7}		(2.9±2.0)×10^{-8}
^{134}Gd	^{130}Sm	0^+	0^+	0	0.046	0.043	[3.780±0.050]	(1.103±0.734)×10^{6}		(6.5±4.3)×10^{-5}
^{135}Gd	^{131}Sm	$(5/2^+)$	$[5/2^+]$	0	0.037	0.033	[3.320±0.050]	(4.370±3.289)×10^{9}		(6.6±5.4)×10^{-8}
^{136}Gd	^{132}Sm	0^+	0^+	0	0.028	0.024	[3.570±0.050]	(3.623±2.554)×10^{7}		(5.5±3.9)×10^{-6}
^{137}Gd	^{133}Sm	$(7/2)^{[+]}$	$(5/2^+)$	2	0.019	0.015	[3.590±0.050]	(1.493±1.045)×10^{8}		(3.1±2.3)×10^{-6}
^{138}Gd	^{134}Sm	0^+	0^+	0	0.010	0.006	[3.150±0.050]	(8.778±6.893)×10^{10}		(1.6±1.4)×10^{-8}
^{139}Gd	^{135}Sm	$[9/2^-]$	$(7/2^+)$	1	0.002	−0.003	[2.801±0.050]	(3.076±2.626)×10^{15}		(7.1±6.2)×10^{-13}
^{135}Tb	^{131}Eu	$(7/2^-)$	$3/2^+$	3	0.058	0.054	[4.020±0.050]	(8.734±5.508)×10^{5}		(2.3±1.7)×10^{-7}
^{136}Tb	^{132}Eu			0	0.048	0.044	[3.650±0.050]	(4.902±3.416)×10^{7}		(7.9±5.5)×10^{-7}
^{137}Tb	^{133}Eu	$[11/2^-]$	$[11/2^-]$	0	0.039	0.035	[3.840±0.050]	(1.576±1.041)×10^{6}		(6.8±4.5)×10^{-5}
^{138}Tb	^{134}Eu			0	0.030	0.026	[3.840±0.050]	(1.846±1.222)×10^{6}		(7.7±5.1)×10^{-5}
^{139}Tb	^{135}Eu	$[11/2^-]$	$[11/2^-]$	0	0.021	0.016	[3.590±0.050]	(9.632±6.808)×10^{7}		(3.6±2.8)×10^{-6}
^{140}Tb	^{136}Eu	(7^+)	(7^+)	0	0.012	0.007	[3.340±0.050]	(1.375±1.040)×10^{10}		(4.2±3.3)×10^{-8}
^{141}Tb	^{137}Eu	$(5/2^-)$	$[11/2^-]$	4	0.004	−0.003	3.180±0.105	(2.451±2.396)×10^{13}		(3.5±3.4)×10^{-10}
^{138}Dy	^{134}Gd	0^+	0^+	0	0.050	0.046	[3.950±0.050]	(1.259±0.818)×10^{6}		(2.8±1.8)×10^{-5}
^{139}Dy	^{135}Gd	$(7/2^+)$	$(5/2^+)$	2	0.041	0.037	[4.320±0.050]	(3.659±2.151)×10^{4}		(3.0±2.3)×10^{-3}
^{140}Dy	^{136}Gd	0^+	0^+	0	0.032	0.028	[3.840±0.050]	(7.023±4.704)×10^{6}		(1.8±1.2)×10^{-5}
^{141}Dy	^{137}Gd	$(9/2^-)$	$(7/2)^{[+]}$	1	0.024	0.019	[3.410±0.050]	(1.194±0.895)×10^{11}		(1.9±1.6)×10^{-9}
^{142}Dy	^{138}Gd	0^+	0^+	0	0.015	0.010	[3.260±0.050]	(3.698±2.881)×10^{11}		(1.7±1.4)×10^{-9}
^{143}Dy	^{139}Gd	$(1/2^+)$	$[9/2^-]$	5	0.007	0.002	[3.040±0.050]	(4.870±4.006)×10^{15}		(4.1±3.6)×10^{-13}
^{140}Ho	^{136}Tb	$[8^+]$		0	0.053	0.048	[4.450±0.050]	(4.452±2.562)×10^{3}		(2.6±2.2)×10^{-4}
^{141}Ho	^{137}Tb	$(7/2^-)$	$[11/2^-]$	2	0.044	0.039	[4.180±0.050]	(1.094±0.677)×10^{6}		(6.2±3.9)×10^{-7}
^{142}Ho	^{138}Tb	(8^+)		0	0.035	0.030	[3.990±0.050]	(2.849±1.850)×10^{6}		(2.8±2.2)×10^{-5}

Continued on next page

Table 2. – continued from previous page

parent	daughter	$J^{\pi}_{\rm P}$ [45]	$J^{\pi}_{\rm D}$ [45]	$\ell_{\rm min}$	$\Delta_{\rm p}$(P)/fm	$\Delta_{\rm p}$(D)/fm	Q_α/MeV [44]	$T^{\rm cal}_\alpha$/s	$T^{\rm exp}_\alpha$/s [45]	$B_{\rm cal}$(%)
^{143}Ho	^{139}Tb	$[11/2^-]$	$[11/2^-]$	0	0.026	0.021	[3.660±0.050]	(6.920±4.909)×10^{8}		(8.7±6.2)×10^{-8}
^{144}Ho	^{140}Tb	(5^-)	(7^+)	3	0.018	0.012	[3.450±0.050]	(6.127±4.595)×10^{11}		(2.9±2.3)×10^{-10}
^{145}Ho	^{141}Tb	$[11/2^-]$	$(5/2^-)$	4	0.010	0.004	3.000±0.110	(9.750±9.632)×10^{16}		(1.1±1.1)×10^{-13}
^{146}Ho	^{142}Tb	(6^-)	1^+	5	0.002	−0.004	[2.896±0.050]	(1.363±1.165)×10^{18}		<10^{-15}
^{142}Er	^{138}Dy	0^+	0^+	0	0.054	0.050	[4.480±0.050]	(9.121±5.271)×10^{3}		(1.7±1.0)×10^{-7}
^{143}Er	^{139}Dy	$[9/2^-]$	$(7/2^+)$	1	0.046	0.041	[3.960±0.050]	(1.506±0.999)×10^{8}		(2.4±1.6)×10^{-7}
^{144}Er	^{140}Dy	0^+	0^+	0	0.037	0.032	[3.800±0.050]	(2.787±1.927)×10^{8}		(2.8±1.9)×10^{-7}
^{145}Er	^{141}Dy	$[1/2^+]$	(9/2-)	5	0.029	0.024	[3.720±0.050]	(1.069±0.757)×10^{11}		(2.1±1.8)×10^{-9}
^{146}Er	^{142}Dy	0^+	0^+	0	0.020	0.015	[3.370±0.050]	(9.339±7.192)×10^{11}		(5.7±5.0)×10^{-10}
^{147}Er	^{143}Dy	$(1/2^+)$	$(1/2^+)$	0	0.013	0.007	3.140±0.040	(2.002±1.454)×10^{14}		(4.3±3.7)×10^{-12}
^{148}Er	^{144}Dy	0^+	0^+	0	0.006	−0.001	2.666±0.013	(2.310±0.809)×10^{19}		<10^{-15}
^{144}Tm	^{140}Ho	(10^+)	$[8^+]$	2	0.056	0.053	[4.580±0.050]	(8.787±5.016)×10^{4}		(4.8±3.7)×10^{-9}
^{145}Tm	^{141}Ho	$(11/2^-)$	$(7/2^-)$	2	0.048	0.044	[4.360±0.050]	(1.506±0.910)×10^{6}		(3.4±2.2)×10^{-10}
^{146}Tm	^{142}Ho	(1^+)	(7^-)	7	0.039	0.035	[3.770±0.050]	(3.417±2.418)×10^{12}		(9.9±7.6)×10^{-12}
^{147}Tm	^{143}Ho	$11/2^-$	$[11/2^-]$	0	0.031	0.026	[3.650±0.050]	(2.239±1.625)×10^{10}		(5.7±4.3)×10^{-9}
^{148}Tm	^{144}Ho	(10^+)	(5^-)	5	0.024	0.018	3.420±0.013	(1.541±0.408)×10^{14}		(5.3±2.7)×10^{-13}
^{149}Tm	^{145}Ho	(11/2-)	$[11/2^-]$	0	0.016	0.010	[2.810±0.050]	(5.336±4.687)×10^{18}		<10^{-15}
^{150}Tm	^{146}Ho	(1^+)	(6^-)	5	0.009	0.002	[2.320±0.050]	(5.770±5.484)×10^{27}		<10^{-15}
^{151}Tm	^{147}Ho	(11/2-)	$(11/2^-)$	0	0.002	−0.005	2.559±0.020	(5.374±3.012)×10^{21}		<10^{-15}
^{148}Yb	^{144}Er	0^+	0^+	0	0.042	0.037	[3.850±0.050]	(2.228±1.550)×10^{9}		(2.2±1.5)×10^{-8}
^{149}Yb	^{145}Er	$(1/2^+)$	$[1/2^+]$	0	0.034	0.029	[3.620±0.050]	(2.258±1.667)×10^{11}		(8.3±7.0)×10^{-10}
^{150}Yb	^{146}Er	0^+	0^+	0	0.026	0.020	[3.260±0.050]	(3.403±2.737)×10^{14}		(5.8±4.7)×10^{-13}
^{151}Yb	^{147}Er	$(1/2^+)$	$(1/2^+)$	0	0.019	0.013	[2.640±0.050]	(6.252±5.692)×10^{21}		<10^{-15}
^{152}Yb	^{148}Er	0^+	0^+	0	0.012	0.006	[2.780±0.050]	(1.051±0.934)×10^{20}		<10^{-15}
^{153}Yb	^{149}Er	[7/2-]	$(1/2^+)$	3	0.001	−0.002	[4.110±0.050]	(4.591±2.997)×10^{8}		(1.6±1.1)×10^{-6}
^{150}Lu	^{146}Tm	(5^-)	(1^+)	5	0.044	0.039	[3.990±0.050]	(9.869±6.718)×10^{10}		(8.9±6.4)×10^{-11}
^{151}Lu	^{147}Tm	$(11/2^-)$	$11/2^-$	0	0.036	0.031	[3.440±0.050]	(3.426±2.661)×10^{13}		(5.8±4.6)×10^{-13}
^{152}Lu	^{148}Tm	(4^-)	(10^+)	7	0.029	0.024	[2.920±0.050]	(2.020±1.761)×10^{22}		<10^{-15}
^{154}Lu	^{150}Tm	(2^-)	(1^+)	1	0.011	0.009	[4.350±0.050]	(1.851±1.146)×10^{7}		(8.8±5.4)×10^{-6}
^{155}Lu	^{151}Tm	$(11/2^-)$	$(11/2^-)$	0	0.002	0.002	5.803±0.003	(2.460±0.701)×10^{-2}	(7.630±0.347)×10^{-2}	
^{153}Hf	^{149}Yb	$[1/2^+]$	$(1/2^+)$	0	0.039	0.034	[3.470±0.050]	(9.484±7.371)×10^{13}		(1.1±0.8)×10^{-12}
^{154}Hf	^{150}Yb	0^+	0^+	0	0.031	0.026	[3.540±0.050]	(2.819±2.155)×10^{13}		(2.4±2.2)×10^{-11}
^{155}Hf	^{151}Yb	$[7/2^-]$	$(1/2^+)$	3	0.021	0.019	[4.950±0.050]	(8.707±4.701)×10^{3}		(1.4±0.8)×10^{-2}
^{156}Hf	^{152}Yb	0^+	0^+	0	0.012	0.012	6.029±0.004	(9.637±0.325)×10^{-2}	(2.377±0.177)×10^{-2}	
^{157}Hf	^{153}Yb	$(7/2^-)$	$[7/2^-]$	0	0.002	0.001	5.880±0.003	(1.829±0.051)×10^{-1}	(1.226±0.063)×10^{-1}	
^{155}Ta	^{151}Lu	$(11/2^-)$	$(11/2^-)$	0	0.041	0.036	[3.760±0.050]	(1.937±1.420)×10^{12}		(4.6±4.1)×10^{-13}
^{156}Ta	^{152}Lu	(2^-)	(4^-)	2	0.030	0.029	[5.140±0.050]	(6.284±3.274)×10^{3}		(2.4±1.3)×10^{-3}
^{157}Ta	^{153}Lu	$1/2^+$	11/2-	5	0.022	0.022	6.355±0.006	(5.120±3.001)×10^{-2}	(1.046±0.041)×10^{-2} [49]	
^{158}Ta	^{154}Lu	(2^-)	(2^-)	0	0.012	0.011	6.124±0.004	(6.404±0.244)×10^{-2}	(5.148±1.048)×10^{-2}	
^{159}Ta	^{155}Lu	$1/2^+$	$(11/2^-)$	5	0.004	0.002	5.681±0.006	220.300±13.302	3.166±0.730	

Continued on next page

Table 2. – continued from previous page

parent	daughter	$J^{\pi}_{\rm P}$ [45]	$J^{\pi}_{\rm D}$ [45]	$\ell_{\rm min}$	$\Delta_{\rm p}$(P)/fm	$\Delta_{\rm p}$(D)/fm	Q_α/MeV [44]	$T^{\rm cal}_\alpha$/s	$T^{\rm exp}_\alpha$/s [45]	$B_{\rm cal}$(%)
^{157}W	^{153}Hf	$(7/2^-)$	$[1/2^+]$	3	0.040	0.039	[5.410±0.050]	(5.818±2.879)×10^2		(6.7±4.0)×10^{-2}
^{158}W	^{154}Hf	0^+	0^+	0	0.031	0.031	6.613±0.003	(2.540±0.062)×10^{-3}	(1.250±0.210)×10^{-3}	
^{159}W	^{155}Hf	$[7/2^-]$	$[7/2^-]$	0	0.023	0.021	6.450±0.004	(0.979±0.032)×10^{-2}	(1.057±0.292)×10^{-2}	
^{160}W	^{156}Hf	0^+	0^+	0	0.013	0.012	6.066±0.005	(2.105±0.087)×10^{-1}	(1.049±0.154)×10^{-1}	
^{161}W	^{157}Hr	$[7/2^-]$	$(7/2^-)$	0	0.005	0.002	5.923±0.004	(8.176±0.278)×10^{-1}	(5.621±0.450)×10^{-1}	
^{159}Re	^{155}Ta	$[1/2^+]$	$(11/2^-)$	5	0.040	0.041	6.760±0.060	(1.727±0.700)×10^{-1}		(2.8±1.1)×10^{-2}
^{160}Re	^{156}Ta	(4^-)	(2^-)	2	0.031	0.030	6.698±0.004	(14.300±0.461)×10^{-3}	(5.607±0.573)×10^{-3}	
^{161}Re	^{157}Ta	$1/2^+$	$1/2^+$	0	0.023	0.022	6.328±0.007	(6.510±0.373)×10^{-2}	¿(3.143±0.007)×10^{-2}	
^{162}Re	^{158}Ta	(2^-)	(2^-)	0	0.015	0.012	6.240±0.005	0.147±1.007	0.115±0.021	
^{163}Re	^{159}Ta	$1/2^+$	$1/2^+$	0	0.006	0.004	6.012±0.008	0.887±0.064	1.250±0.336	
^{161}Os	^{157}W	$(7/2^-)$	$(7/2^-)$	0	0.040	0.040	7.066±0.012	(5.722±0.514)×10^{-4}	(6.400±0.600)×10^{-4}	
^{162}Os	^{158}W	0^+	0^+	0	0.032	0.031	6.767±0.003	(4.305±0.104)×10^{-3}	(2.100±0.100)×10^{-3}	
^{163}Os	^{159}W	$7/2^-$	$[7/2^-]$	0	0.024	0.023	6.677±0.008	(9.099±0.608)×10^{-3}	(5.500±0.600)×10^{-3}	
^{164}Os	^{160}W	0^+	0^+	0	0.016	0.013	6.479±0.005	(3.640±0.160)×10^{-2}	(2.143±0.102)×10^{-2} [49]	
^{165}Os	^{161}W	$(7/2^-)$	$[7/2^-]$	0	0.008	0.005	6.335±0.006	(13.440±0.661)×10^{-2}	(7.900±0.509)×10^{-2}	
^{166}Os	^{162}W	0^+	0^+	0	0.001	−0.003	6.143±0.003	(5.740±0.174)×10^{-1}	(3.071±0.624)×10^{-1}	
^{164}Ir	^{160}Re	$[2^-]$	(4^-)	2	0.033	0.031	[6.970±0.050]	(1.222±0.443)×10^{-2}		9.4±3.4
^{165}Ir	^{161}Re	$[1/2^+]$	$1/2^+$	0	0.025	0.023	6.820±0.050	(7.463±2.783)×10^{-3}		<(1.6±0.6)×10^{-2}
^{166}Ir	^{162}Re	(2^-)	(2^-)	0	0.017	0.015	6.722±0.006	(1.654±0.074)×10^{-2}	(1.138±0.273)×10^{-2}	
^{167}Ir	^{163}Re	$1/2^+$	$1/2^+$	0	0.009	0.006	6.505±0.003	(7.848±0.175)×10^{-2}	(6.835±0.458)×10^{-2}	
^{168}Ir	^{164}Re	(2^-)	(2^-)	0	0.002	−0.003	6.381±0.009	0.262±0.019	0.230±0.050	
^{166}Pt	^{162}Os	0^+	0^+	0	0.034	0.032	7.286±0.015	(5.082±0.558)×10^{-4}	(3.000±1.000)×10^{-4}	
^{167}Pt	^{163}Os	$[7/2^-]$	$7/2^-$	0	0.026	0.024	7.160±0.050	(15.350±5.410)×10^{-4}	(8.000±1.600)×10^{-4}	
^{168}Pt	^{164}Os	0^+	0^+	0	0.019	0.016	6.990±0.003	(3.847±0.090)×10^{-3}	(2.020±0.100)×10^{-3}	
^{169}Pt	^{165}Os	$(7/2^-)$	$(7/2^-)$	0	0.011	0.008	6.858±0.005	(12.390±0.500)×10^{-3}	(6.990±0.090)×10^{-3} [49]	
^{170}Pt	^{166}Os	0^+	0^+	0	0.004	0.001	6.707±0.003	(3.246±0.084)×10^{-2}	(1.408±0.051)×10^{-2} [49]	
^{169}Au	^{165}Ir	$[1/2^+]$	$[1/2^+]$	0	0.027	0.025	[7.380±0.050]	(6.932±2.368)×10^{-4}		24.5±8.3
^{170}Au	^{166}Ir	(2^-)	(2^-)	0	0.020	0.017	7.177±0.015	(0.338±0.038)×10^{-2}	(1.757±1.643)×10^{-2}	
^{171}Au	^{167}Ir	$(1/2^+)$	$1/2^+$	0	0.013	0.009	7.085±0.011	(5.330±9.432)×10^{-3}		0.4±0.1
^{172}Au	^{168}Ir	(2^-)	(2^-)	0	0.006	0.002	6.923±0.010	(2.311±0.186)×10^{-2}	(2.300±0.500)×10^{-2} [49]	
^{171}Hg	^{167}Pt	$[3/2^-]$	$[7/2^-]$	2	0.029	0.026	7.668±0.015	(11.350±1.180)×10^{-4}	(7.000±3.000)×10^{-5}	
^{172}Hg	^{168}Pt	0^+	0^+	0	0.022	0.019	7.524±0.006	(4.938±0.214)×10^{-4}	(2.310±0.090)×10^{-4}	
^{173}Hg	^{169}Pt	$[3/2^-]$	$(7/2^-)$	2	0.015	0.011	7.378±0.004	(86.550±2.791)×10^{-4}	(8.000±0.800)×10^{-4}	
^{174}Hg	^{170}Pt	0^+	0^+	0	0.008	0.004	7.233±0.006	(3.929±0.176)×10^{-3}	(2.000±0.400)×10^{-3}	
^{175}Hg	^{171}Pt	$(7/2^-)$	$7/2^-$	0	0.001	−0.002	7.072±0.005	(1.758±0.063)×10^{-2}	(1.060±0.040)×10^{-2} [49]	
^{176}Tl	^{172}Au	(3^-)	(2^-)	2	0.010	0.006	7.470±0.090	(1.972±1.158)×10^{-2}		56.2±43.8
^{177}Tl	^{173}Au	$(1/2^+)$	$(1/2^+)$	0	0.003	−0.001	7.067±0.007	(4.898±0.275)×10^{-2}	(2.672±1.161)×10^{-2}	
^{178}Pb	^{174}Hg	0^+	0^+	0	0.011	0.008	7.790±0.014	(6.080±0.591)×10^{-4}	(2.300±1.500)×10^{-4}	
^{179}Pb	^{175}Hg	$(9/2^-)$	$(7/2^-)$	2	0.005	0.001	7.598±0.020	(14.260±2.010)×10^{-3}	(3.900±1.100)×10^{-3}	

calculations based on the Skyrme-SLy4 interaction rather than the M3Y interaction. For the ^{115}Xe isotope, however, the difference between $T_\alpha^{\rm cal}$ and $T_\alpha^{\rm exp}$ is four orders of magnitude. To check this result, we calculated the half-life based on the Skyrme-SLy4 and got a similar difference, $T_\alpha^{\rm cal}$(Skyrme-SLy4)= 0.645±0.271 $\times 10^{10}$ s. This difference could be due to uncertainty in the observed half-life and the corresponding low intensity, as these measurements are relatively old [45].

The main observed decay modes for the 129 neutron-deficient nuclei investigated that have no detected α-decays are β^+ (106 nuclei (82.2%)) and proton (23 nuclei (17.8%)) decays [45]. Proton-decay was confirmed as the main decay mode of the odd Z ^{113}Cs, ^{121}Pr, ^{130,131}Eu, ^{135}Tb, ^{141}Ho, ^{145,146}Tm, $^{155.156}$Ta, ^{171}Au and ^{176}Tl nuclei, with B(p) $\sim$ 100 %. These nuclei show relative larger calculated $\Delta_{\rm p}$ and have relative smaller isospin asymmetry than their isotopes. As seen in Table 2, among the investigated α-decays of these 129 nuclei, the five ground-state to ground-state decays of ^{107}I, ^{113}Ba, ^{164}Ir, ^{169}Au and ^{176}Tl yield estimated percentage branching greater than 1%. Sixteen decay modes yield branching ratio 10^{-5} % $<B_{\rm cal}$ <1%. Most of the investigated decays, 8 decays (62 %), exhibit smaller intensity in the range of 10^{-15} % $<B_{\rm cal}$ $<10^{-5}$ %. The smallest indicated percentage branching of an observed decay is of the order of 10^{-15} % [45]. The remaining 28 decays yield extremely small branching ratios of less than 10^{-15} %.

4 Summary and conclusions

First, we discussed the behaviour of the different contributions of the interaction potential between the emitted α-particle and the daughter nucleus with the change of the proton-skin thickness $\Delta_{\rm p}$ of the neutron-deficient daughter nucleus. We then investigated the influence of this behavior on the α-decay process. Finally, we explored the ground-state to ground-state α-decay of the neutron-deficient nuclei with A =105–179 (Z =52–82, N =53–97) as main, competing, or minor decay mode. Our results indicate that increasing the proton-skin thickness of the daughter nucleus increases the width of the internal pocket of the interaction potential and shifts down its lowest point. This decreases the assault frequency. More importantly, the increasing of $\Delta_{\rm p}$ produces a lower Coulomb barrier with a relatively thinner barrier width. The radius of the Coulomb barrier slightly increases. Consequently, the penetration probability increases with increasing $\Delta_{\rm p}$. The enhancement in the penetration probability due to increasing $\Delta_{\rm p}$ is more prominent in the decay process than the relative decrease in the assault frequency. The net effect of these two contradicting factors is to enhance the decay width, leading to a shorter half-life. It is then essential to employ the precise $\Delta_{\rm p}$ to predict the correct estimation of the half-life. Along the same isotopic chain, while the Q_α-values increase linearly with increasing proton-skin thickness of the parent nuclei, their half-lives decrease exponentially with $\Delta_{\rm p}$. Therefore, the stability of the nucleus decreases with increasing proton-skin thickness. Between the β^+ and proton decays, the α-decay comes as the second preferred decay mode for neutron-deficient nuclei. It is experimentally observed and theoretically indicated for 85% of the investigated nuclei.

References

1 Sarrigure, M. K. Gaidaro, E. Moya de Guerr, and A. N. Antonov, Phys. Rev. C, **76**: 044322 (2007)
2 M. Warda, X. Viñas, X. Roca-Maza, and M. Centelles, Phys. Rev. C, **81**: 054309 (2010)
3 N. Fukunishi, T. Otsuka, and I. Tanihata, Phys. Rev. C, **48**: 1648 (1993)
4 W. M. Seif, Nucl. Phys. A, **878**: 14 (2012)
5 B. Alex Brown, Phys. Rev. Lett., **85**: 5296 (2000)
6 X. Roca-Maza, M. Centelles, X. Viñas, and M. Warda, Phys. Rev. Lett., **106**: 252501 (2011)
7 C. J. Horowitz and J. Piekarewicz, Phys. Rev. Lett., **86**: 5647 (2001)
8 E. Rutherford and H. Geiger, Proc. R. Soc. London, Ser. A., **81**: 162 (1908)
9 G. Gamow, Z. Phys., **51**: 204 (1928)
10 B. Blank et al, Phys. Rev. C, **93**: 061301(R) (2016)
11 B. Sumikam et al, Phy. Rev. C, **95**: 051601(R) (2017)
12 H. Badran et al, Phys. Rev. C, **94**: 054301 (2016)
13 W. M. Seif, M. Shalaby, and M. F. Alrakshy, Phys. Rev. C, **84**: 064608 (2011)
14 W. M. Seif, Phys. Rev. C, **74**: 034302 (2006)
15 Chang Xu, Zhongzhou Ren, and Yanqing Guo, Phys. Rev. C, **78**: 044329 (2008)
16 W. M. Seif, M. Ismail, A. I. Refaie, and Laila H. Amer, J. Phys. G: Nucl. Part. Phys., **43**: 075101 (2016)
17 M. Ismail, W. M. Seif, A. Adel, and A. Abdurrahman, Nucl. Phys. A, **958**: 202 (2017)
18 W. M. Seif, Phys. Rev. C, **91**: 014322 (2015); J. Phys. G: Nucl. Part. Phys., **40**: 105102 (2013)
19 Dongdong Ni and Zhongzhou Ren, J. Phys. G: Nucl. Part. Phys., **37**: 035104 (2010)
20 W. M. Seif, M. M. Botros, and A. I. Refaie, Phys. Rev. C, **92**: 044302 (2015)
21 W. M. Seif, M. Ismail, and E. T. Zeini, J. Phys. G: Nucl. Part. Phys., **44**: 055102 (2017)
22 S. Peltonen, D. S. Delion, and J. Suhonen, Phys. Rev. C, **75**: 054301 (2007)
23 Y. Qian, Z. Ren, and D. Ni, Nucl. Phys. A, **866**:1 (2011)
24 M. Ismail, W. M. Seif, and A. Abdurrahman, Phys. Rev. C, **94**: 024316 (2016)
25 Chang Xu, Zhongzhou Ren, and Jian Liu, Phys. Rev. C, **90**: 064310 (2014)
26 W. M. Seif, N. V. Antonenko, G. G. Adamian, and Hisham Anwer, Phys. Rev. C, **96**: 054328 (2017)
27 Dongdong Ni and Zhongzhou Ren, Phys. Rev. C, **93**: 054318 (2016)
28 G. R. Satchler, W. G. Love, Phys. Rep., **55**: 183 (1979)
29 G. Bertsch, J. Borysowicz, H. McManus and W. G. Love, Nucl.

Phys. A, **284**: 399 (1977)
30 D. T. Khoa,W. von Oertzen, and A. A. Ogloblin, Nucl. Phys. A, **602**: 98 (1996)
31 A. M. Kobos, B. A. Brown, R. Lindsay and G. R. Satchler, Nucl. Phys. A, **425**: 205 (1984)
32 M. Ismail, W. M. Seif, and H. EL Gebaly, Phys. Lett. B, **563**: 53 (2003)
33 M. Ismail, W. M. Seif, and M. M. Botros, Nucl. Phys. A, **828**: 333 (2009); Int. J. Mod. Phys. E, **25**: 1650026 (2016)
34 M. Ismail and W. M. Seif, Phys. Rev. C, **81**: 034607 (2010)
35 P. Möller, A. J. Sierk, T. Ichikawa, and H. Sagawa, At. Data Nucl. Data Tables, **109-110**: 1 (2016)
36 P. Möller, J. R. Nix, W. D. Myers, and W. J. Swiatecki, At. Data Nucl. Data Tables, **59** 185 (1995)
37 W. M. Seif and Hesham Mansour, Int. J. Mod. Phys. E, **24**: 1550083 (2015)
38 P. -G. Reinhard, *Computational Nuclear Physics*, Vol. 1, edited by K. Langanke, J. A. Maruhn, and S. E. Koonin (Springer-Verlag, Berlin, 1990) p. 28.
39 E. Chabanat, E. Bonche, E. Haensel, J. Meyer, and R. Schaeffer, Nucl. Phys. A, **35**: 231 (1998)
40 B. Buck, A. C. Merchant, and S. M. Perez, Phys. Rev. C, **45,** 2247 (1992)
41 N. G. Kelkar and H. M. Castañeda, Phys. Rev. C, **76**: 064605 (2007)
42 B. Buck, J. C. Johnston, A. C. Merchant, and S. M. Perez, Phys. Rev. C, **53**: 2841 (1996)
43 K. Wildermuth and Y. C. Tang, *A Unified Theory of the Nucleus* (Academic, New York, 1977)
44 Meng Wang, G. Audi, F. G. Kondev, W. J. Huang, S. Naimi, and Xing Xu, Chin. Phys. C, **41**: 030003 (2017)
45 G. Audi, F. G. Kondev, Meng Wang, W. J. Huang, and S. Naimi, Chin. Phys. C **41**: 030001 (2017)
46 B. K. Agrawal, S. Shlomo, and V. Kim Au, Phys. Rev. C, **68**: 031304(R) (2003)
47 D. Vautherin and D. M. Brink, Phys. Rev. C, **5**: 626 (1972)
48 H. R. Jaqaman, A. Z. Mekjian, and I.. Zamick, Phys. Rev. C, **29**: 2067 (1984)
49 Jagdish K. Tuli, Nuclear Wallet Cards, 8^{th} ed. (2011), http://www.nndc.bnl.gov http://www.nndc.bnl.gov